

Asynchronous Distributed Gaussian Process Regression for Online Learning and Dynamical Systems: Complementary Document

Zewen Yang, Xiaobing Dai, Sandra Hirche

I. EXTENDED INTRODUCTION AND RELATED WORK

In the realm of real-time online Gaussian Process (GP) regression, continuously collecting the training data becomes impractical for dynamic systems due to the constraints in physical storage space and the escalating computational burden [2]. Instead of employing the entire dataset for prediction, several approximation techniques prove instrumental. These include sparse approximation methods such as sparse subset-of-data [3], [4] and sparse kernel methods [5], as well as projections/embedding approaches [6]. Moreover, local approximation methods, such as the naive local experts, the mixture of experts, and the product of experts, present viable alternatives. For an in-depth exploration of these approximation techniques, comprehensive discussions can be found in review papers [7], [8].

A. Local Approximation Gaussian Process

Prominently, cooperative learning within distributed systems falls under the purview of local approximation, where each subsystem, functioning as a computation node, assumes the role of an expert. A common instance in this context is the mixture of experts (MOE) method [9]–[11], where each model’s prediction is weighted by the predefined factor, even with the selection of experts. To alleviate this limitation, various techniques have been explored to enhance aggregate weights. The product of experts (POE), leveraging the posterior mean of GP models [12], [13], and the generalized product of experts (GPOE), which incorporates the difference in entropy between the prior and posterior [14]. Moreover, combining sparse GP and barycenters, correlated POE is introduced in [15], [16]. In contrast to the POE framework, both the Bayesian committee machine (BCM) [17] and its robust variant, robust BCM (RBCM) [18], integrate the GP prior. However, these models exhibit limitations in sustaining consistent predictions as the training dataset undergoes continuous expansion. Notably, the generalized RBCM, reliant on dataset sharing among models, introduces challenges in the context of distributed online learning [19] under limited

communication or with constrained bandwidth. Additionally, the investigation into the nested pointwise aggregation of experts has been undertaken [20], [21]. Nevertheless, the application of pointwise aggregation across the entirety of the training dataset proves unattainable within distributed systems. Therefore, the discernible increase in prediction time poses substantial practical challenges, particularly in real-time dynamical systems.

B. Agent-based Gaussian Process

Distributed learning finds prominent application in multi-agent systems (MASs), where each individual agent is treated as a central node, and their neighboring agents are considered computational nodes. Consequently, joint predictions are aggregated within a cooperative learning framework to enhance individual predictions [22], [23].

Several efforts have been dedicated to implementing distributed Gaussian Process (DGP) methodologies within MASs. Effective strategies include employing the POE to refine aggregation weights [24] and applying the dynamical average consensus algorithm to accelerate joint prediction convergence [25]. Nevertheless, these endeavors demonstrate limitations in addressing concerns specific to online learning challenges. In situations where GP models lack the capability to dynamically update with new observations or measurements, a potential constraint arises, as the data-driven model may encounter difficulties in adapting to a dynamic and evolving environment. The works of [26]–[30] have strategically addressed this crucial gap, emphasizing the necessity of integrating online data to ensure the adaptability of DGP in dynamic environments.

While the data fusion method is characterized as decentralized in [31], [32], it is crucial to emphasize that this approach entails the need for the central server to access a subset of data, implying the amalgamation of datasets. However, this requirement poses challenges for its direct applicability in distributed systems. Similarly, the nested pointwise aggregation approach, as discussed in [33], relies on data sharing, a condition that may not be conducive to certain distributed scenarios. A strategy proposed by [34] introduces a finite-dimensional approximation of GP for MAS observation, aiming to reduce computational and communication demands. However, this method mandates the collection of all data, despite a reduction in data dimensionality. The work in [35] introduced an algorithm designed to minimize communication

Zewen Yang, Xiaobing Dai and Sandra Hirche are with the Chair of Information-oriented Control (ITR), School of Computation, Information and Technology (CIT), Technical University of Munich (TUM), 80333 Munich, Germany (email: zewen.yang@tum.de, xiaobing.dai@tum.de, hirche@tum.de).

This is a complementary document for the paper titled with “Asynchronous Distributed Gaussian Process Regression for Online Learning and Dynamical Systems” [1].

costs while simultaneously achieving low distortion in the reconstruction of the Gram matrix within distributed systems. However, these approaches still necessitate data sharing.

In the realm of Gaussian graphical models, [36] introduces an innovative approach for aggregating Gaussian experts by identifying significant violations of conditional independence. The dependency among experts is ascertained through a Gaussian graphical model, which provides the precision matrix leading to an improved aggregation strategy. Meanwhile, [37] presents a graph spectrum-based Gaussian process for predicting signals defined on graph nodes. This approach incorporates a highly adaptive kernel that embraces various graph signal structures through a flexible polynomial function in the graph spectral domain.

In the scenario where each agent is equipped with functional sensors, [38] devises a distributed navigation strategy, considering the limited communication range among agents. Furthermore, [39] introduces an approach for active sensing model learning tailored for multi-agent coordination. This methodology aims to discern the highest peak within an unknown environmental field while incorporating strategies for collision avoidance. Similarly, in [39]–[41], the online learning approaches for field mapping and environmental modeling are proposed through the application of distributed Gaussian processes.

II. PROOFS FOR PREDICTION PERFORMANCE

A. Proof of Lemma 3

Using the triangular inequality, the delayed prediction error is bounded as

$$\begin{aligned} & |f(\mathbf{x}(t)) - \mu_i(\mathbf{x}(t_i^k))| \\ & \leq |f(\mathbf{x}(t)) - f(\mathbf{x}(t_i^k))| + |f(\mathbf{x}(t_i^k)) - \mu_i(\mathbf{x}(t_i^k))| \quad (1) \\ & \leq |f(\mathbf{x}(t)) - f(\mathbf{x}(t_i^k))| + \beta\sigma_i(\mathbf{x}(t_i^k)), \end{aligned}$$

where the second inequality is obtained by using the result in Lemma 2. Moreover, using the reproducing property of κ [42], the first term in (1) becomes

$$\begin{aligned} & |f(\mathbf{x}(t)) - f(\mathbf{x}(t_i^k))|^2 \quad (2) \\ & \leq \|f\|_\kappa^2 (\kappa(\mathbf{x}(t), \mathbf{x}(t)) + \kappa(\mathbf{x}(t_i^k), \mathbf{x}(t_i^k)) - 2\kappa(\mathbf{x}(t), \mathbf{x}(t_i^k))). \end{aligned}$$

Furthermore, considering $\|f\|_\kappa \leq \Gamma$ and

$$|\kappa(\cdot, \mathbf{x}(t)) - \kappa(\cdot, \mathbf{x}(t_i^k))| \leq L_\kappa d(\mathbf{x}(t) - \mathbf{x}(t_i^k)), \quad (3)$$

inequality (2) is further bounded by

$$\begin{aligned} |f(\mathbf{x}(t)) - f(\mathbf{x}(t_i^k))|^2 & \leq 2\|f\|_\kappa^2 L_\kappa d(\mathbf{x}(t) - \mathbf{x}(t_i^k)) \quad (4) \\ & \leq 2L_\kappa^2 d(\mathbf{x}(t) - \mathbf{x}(t_i^k)). \end{aligned}$$

Apply (4) into (1), then the boundness of the delayed prediction error as $\eta_i^k(t)$ in the lemma is derived.

B. Proof of Theorem 7

With the design of aggregation weights $\omega_k^i(t)$ and $\omega_m(t)$, it is easy to see

$$\sum_{i=1}^M \sum_{k=0}^{\bar{k}_i(t)} \omega_k^i(t) + \omega_m(t) = 1. \quad (5)$$

Combining with the triangular inequality, the prediction error is bounded by

$$\begin{aligned} |f(\mathbf{x}(t)) - \hat{f}(\mathbf{x}(t))| & \leq \sum_{i=1}^M \sum_{k=0}^{\bar{k}_i(t)} \omega_k^i(t) |f(\mathbf{x}(t)) - \mu_i(\mathbf{x}(t_i^k))| \\ & \quad + \omega_m(t) |f(\mathbf{x}(t)) - m(\mathbf{x}(t))| \quad (6) \\ & \leq \sum_{i=1}^M \sum_{k=0}^{\bar{k}_i(t)} \omega_k^i(t) \eta_i^k(t) + \omega_m(t) \beta\sigma_f, \end{aligned}$$

where the second inequality is derived using the result in Lemma 3 and $|f(\mathbf{x}(t)) - m(\mathbf{x}(t))| \leq \beta\sigma_f$. Note that maximal $\bar{\mathcal{I}}$ previous predictions will be used, combining with the deterministic error bound for the prior mean, the second inequality holds using union bound. Additionally, applying the expression of aggregation weights, the prediction error is further bounded by

$$\begin{aligned} & |f(\mathbf{x}(t)) - \hat{f}(\mathbf{x}(t))| \quad (7) \\ & \leq \omega^2(t) \left(\sum_{i=1}^M \sum_{k=0}^{\bar{k}_i(t)} \rho_k^i(t) (\eta_i^k(t))^{-1} + (1 - \rho(t)) (\beta\sigma_f)^{-1} \right) \end{aligned}$$

with

$$\rho(t) = \sum_{i=1}^M \sum_{k=0}^{\bar{k}_i(t)} \rho_k^i(t). \quad (8)$$

Then, (7) is further bounded by

$$\begin{aligned} & |f(\mathbf{x}(t)) - \hat{f}(\mathbf{x}(t))| \\ & \leq \frac{\sum_{i=1}^M \sum_{k=0}^{\bar{k}_i(t)} \rho_k^i(t) (\eta_i^k(t))^{-1} + (1 - \rho(t)) (\beta\sigma_f)^{-1}}{\sum_{i=1}^M \sum_{k=0}^{\bar{k}_i(t)} \rho_k^i(t) (\eta_i^k(t))^{-2} + (1 - \rho(t)) (\beta\sigma_f)^{-2}} \quad (9) \\ & = \frac{\sum_{i=1}^M \sum_{k=0}^{\bar{k}_i(t)} \rho_k^i(t) ((\eta_i^k(t))^{-1} - (\beta\sigma_f)^{-1}) + (\beta\sigma_f)^{-1}}{\sum_{i=1}^M \sum_{k=0}^{\bar{k}_i(t)} \rho_k^i(t) ((\eta_i^k(t))^{-2} - (\beta\sigma_f)^{-2}) + (\beta\sigma_f)^{-2}}. \end{aligned}$$

Considering the definition of $\rho_k^i(t)$, it has $\rho_k^i(t) = 0$ if $\eta_i^k(t) \geq \beta\sigma_f$, such that $(\eta_i^k(t))^{-1} - (\beta\sigma_f)^{-1} > 0$. Apply Cauchy-Schwarz inequality, then

$$\begin{aligned} & \left(\sum_{i=1}^M \sum_{k=0}^{\bar{k}_i(t)} \rho_k^i(t) ((\eta_i^k(t))^{-1} - (\beta\sigma_f)^{-1}) + (\beta\sigma_f)^{-1} \right)^2 \\ & \leq \left(\sum_{i=1}^M \sum_{k=0}^{\bar{k}_i(t)} \rho_k^i(t) + 1 - \rho(t) \right) \quad (10) \\ & \quad \times \left(\sum_{i=1}^M \sum_{k=0}^{\bar{k}_i(t)} \rho_k^i(t) ((\eta_i^k(t))^{-1} - (\beta\sigma_f)^{-1})^2 + (\beta\sigma_f)^{-2} \right) \\ & = \sum_{i=1}^M \sum_{k=0}^{\bar{k}_i(t)} \rho_k^i(t) ((\eta_i^k(t))^{-1} - (\beta\sigma_f)^{-1})^2 + (\beta\sigma_f)^{-2}. \end{aligned}$$

Additionally, considering

$$((\eta_i^k(t))^{-1} - (\beta\sigma_f)^{-1})^2 \quad (11)$$

$$\begin{aligned} & \leq ((\eta_i^k(t))^{-1} - (\beta\sigma_f)^{-1}) ((\eta_i^k(t))^{-1} + (\beta\sigma_f)^{-1}) \quad (12) \\ & = (\eta_i^k(t))^{-2} - (\beta\sigma_f)^{-2}, \end{aligned}$$

one has

$$\begin{aligned} & \left(\sum_{i=1}^M \sum_{k=0}^{\bar{k}_i(t)} \rho_k^i(t) ((\eta_i^k(t))^{-1} - (\beta\sigma_f)^{-1}) + (\beta\sigma_f)^{-1} \right)^2 \\ & \leq \sum_{i=1}^M \sum_{k=0}^{\bar{k}_i(t)} \rho_k^i(t) ((\eta_i^k(t))^{-2} - (\beta\sigma_f)^{-2}) + (\beta\sigma_f)^{-2}. \end{aligned} \quad (13)$$

Therefore, the prediction error is bounded by

$$\begin{aligned} & |f(\mathbf{x}(t)) - \hat{f}(\mathbf{x}(t))| \quad (14) \\ & \leq \frac{\sqrt{\sum_{i=1}^M \sum_{k=0}^{\bar{k}_i(t)} \rho_k^i(t) ((\eta_i^k(t))^{-2} - (\beta\sigma_f)^{-2}) + (\beta\sigma_f)^{-2}}}{\sum_{i=1}^M \sum_{k=0}^{\bar{k}_i(t)} \rho_k^i(t) ((\eta_i^k(t))^{-2} - (\beta\sigma_f)^{-2}) + (\beta\sigma_f)^{-2}} \\ & = \left(\sum_{i=1}^M \sum_{k=0}^{\bar{k}_i(t)} \rho_k^i(t) ((\eta_i^k(t))^{-2} - (\beta\sigma_f)^{-2}) + (\beta\sigma_f)^{-2} \right)^{-1/2} \\ & = \omega(t), \end{aligned} \quad (15)$$

considering the definition of $\omega(t)$ in (12) in the main context.

C. Proof of Corollary 8

Considering the monotonic increasing of $\omega(t)$ w.r.t $\eta_i^k(t)$ for $\forall i = 1, \dots, M$ from (12) in the main context and recalling $\eta_i^k(t) < \beta\sigma_f$ from the management of information set in Algorithm 1, the time-varying prediction bound $\omega(t)$ is further bounded by

$$\begin{aligned} \omega(t) & \leq \left(\sum_{i=1}^M \sum_{k=0}^{\bar{k}_i(t)} \rho_k^i(t) ((\beta\sigma_f)^{-2} - (\beta\sigma_f)^{-2}) + (\beta\sigma_f)^{-2} \right)^{-\frac{1}{2}} \\ & = \beta\sigma_f, \end{aligned} \quad (16)$$

which concludes the proof.

III. PROOF FOR CONTROL PERFORMANCE IN THEOREM 9

Recall the error dynamics in (23) in the main context as

$$\dot{e}(t) = \mathbf{A}e(t) + \mathbf{b}(f(\mathbf{x}(t)) - \hat{f}(\mathbf{x}(t))). \quad (17)$$

We have the solution of e written as

$$\begin{aligned} e(t) & = \exp(\mathbf{A}(t - t_0)) e(t_0) \\ & + \int_{t_0}^t \exp(\mathbf{A}(t - \tau)) \mathbf{b} \left(f(\mathbf{x}(\tau)) - \hat{f}(\mathbf{x}(\tau)) \right) d\tau \\ & \leq \|\exp(\mathbf{A}(t - t_0))\| \|e(t_0)\| \quad (18) \\ & + \int_{t_0}^t \|\exp(\mathbf{A}(t - \tau))\| \|f(\mathbf{x}(\tau)) - \hat{f}(\mathbf{x}(\tau))\| d\tau. \end{aligned}$$

Using the eigenvalue decomposition, the matrix \mathbf{A} defined in (22) in the main context is formulated as

$$\mathbf{A} = \mathbf{Q}\mathbf{\Lambda}\mathbf{Q}^{-1}, \quad (19)$$

where $\mathbf{\Lambda} = \text{diag}(\Lambda_1, \dots, \Lambda_n)$ is a diagonal matrix composed of all eigenvalues $\Lambda_i \in \mathbb{R}_{<0}, \forall i = 1, \dots, n$ of \mathbf{A} . Moreover, referring to [43], it has

$$\begin{aligned} \|\exp(\mathbf{A}t)\| & = \|\mathbf{Q}\exp(\mathbf{\Lambda}t)\mathbf{Q}^{-1}\| \leq \|\mathbf{Q}\| \|\exp(\mathbf{\Lambda}t)\| \|\mathbf{Q}^{-1}\| \\ & \leq \|\mathbf{Q}\| \|\mathbf{Q}^{-1}\| \exp(\bar{\Lambda}t), \end{aligned} \quad (20)$$

where $\bar{\Lambda} = \max_{i=1, \dots, n} \Lambda_i$ is the maximal value of eigenvalues Λ_i . Considering the prediction error bound in Theorem 7, then Eq. (18) is further derived as

$$\begin{aligned} e(t) & \leq \exp(\bar{\Lambda}(t - t_0)) \|\mathbf{Q}\| \|\mathbf{Q}^{-1}\| \|e(t_0)\| \\ & + \|\mathbf{Q}\| \|\mathbf{Q}^{-1}\| \int_{t_0}^t \exp(\bar{\Lambda}(t - \tau)) \omega(\tau) d\tau \quad (21) \\ & \leq \exp(\bar{\Lambda}(t - t_0)) \|\mathbf{Q}\| \|\mathbf{Q}^{-1}\| \|e(t_0)\| \\ & + \|\mathbf{Q}\| \|\mathbf{Q}^{-1}\| \bar{\omega} \int_{t_0}^t \exp(\bar{\Lambda}(t - \tau)) d\tau, \end{aligned}$$

where $\bar{\omega} = \max_{t \in \mathbb{R}_{\geq 0}} \omega(t)$. Due to the fact that

$$\begin{aligned} \int_{t_0}^t \exp(\bar{\Lambda}(t - \tau)) d\tau & = -\bar{\Lambda}^{-1} \exp(\bar{\Lambda}(t - \tau)) \Big|_{t_0}^t \quad (22) \\ & = -\bar{\Lambda}^{-1} (1 - \exp(\bar{\Lambda}(t - t_0))), \end{aligned}$$

the tracking error bound

$$\begin{aligned} e(t) & \leq \exp(\bar{\Lambda}(t - t_0)) \|\mathbf{Q}\| \|\mathbf{Q}^{-1}\| \|e(t_0)\| \quad (23) \\ & - (1 - \exp(\bar{\Lambda}(t - t_0))) \|\mathbf{Q}\| \|\mathbf{Q}^{-1}\| \bar{\Lambda}^{-1} \bar{\omega}. \end{aligned}$$

Therefore, the ultimate tracking error bound is written as

$$\lim_{t \rightarrow \infty} e(t) \leq -\|\mathbf{Q}\| \|\mathbf{Q}^{-1}\| \frac{\bar{\omega}}{\bar{\Lambda}} = \|\mathbf{Q}\| \|\mathbf{Q}^{-1}\| \frac{\bar{\omega}}{|\bar{\Lambda}|}, \quad (24)$$

by considering the Hurwitz \mathbf{A} inducing $\bar{\Lambda} < 0$, which concludes the proof.

IV. LIPSCHITZ CONTINUITY OF KERNELS

The Lipschitz constant and corresponding distance definition is summarized in Table I, whose results are proven in the following subsections.

A. Proof of Lemma 4 for SE Kernel

Consider the distance function as

$$d_{SE} = \|\mathbf{x} - \mathbf{x}'\|, \quad (25)$$

the derivative of κ_{SE} w.r.t d_{SE} is

$$\begin{aligned} \nabla_{d_{SE}(x, x')} \kappa(x, x') & = \sigma^2 \nabla_{d_{SE}(x, x')} \exp\left(-\frac{d_x^2(x, x')}{2l^2}\right) \quad (26) \\ & = -\sigma^2 \exp\left(-\frac{d_x^2(x, x')}{2l^2}\right) \frac{d_x(x, x')}{l^2}. \end{aligned}$$

Then its second derivative is written as

$$\begin{aligned} & \nabla_{d_{SE}(x, x')} (|\nabla_{d_{SE}(x, x')} \kappa(x, x')|) \\ & = \nabla_{d_x(x, x')} \left(\sigma^2 \exp\left(-\frac{d_x^2(x, x')}{2l^2}\right) \frac{d_x(x, x')}{l^2} \right) \\ & = \left(-\sigma^2 \exp\left(-\frac{d_x^2(x, x')}{2l^2}\right) \frac{d_x(x, x')}{l^2} \frac{d_x(x, x')}{l^2} \right) \quad (27) \\ & + \left(\sigma^2 \exp\left(-\frac{d_x^2(x, x')}{2l^2}\right) \frac{1}{l^2} \right) \\ & = \frac{\sigma^2}{l^2} \exp\left(-\frac{d_x^2(x, x')}{2l^2}\right) \left(-\frac{d_x^2(x, x')}{l^2} + 1 \right) \end{aligned}$$

As the maximum value of $|\nabla_{d_{SE}(x, x')} \kappa(x, x')|$, i.e., its the upper bound, is achieved by letting Eq. (27) to be zero.

Name	Kernel	Distance function	Lipschitz constants
Linear	$\sigma_l^2(\mathbf{x} - \mathbf{c})^T(\mathbf{x}' - \mathbf{c}) + \sigma_b^2$	$(\mathbf{x} - \mathbf{c})^T(\mathbf{x}' - \mathbf{c})$	σ_l^2
SE	$\sigma_f^2 \exp(-\ \mathbf{x} - \mathbf{x}'\ ^2 / (2\sigma_l^2))$	$\ \mathbf{x} - \mathbf{x}'\ $	$\sigma_f^2 \sigma_l^{-1} \exp(-0.5)$
ARD-SE	$\sigma_f^2 \exp(-(\mathbf{x} - \mathbf{x}')^T \Sigma_L^{-2} (\mathbf{x} - \mathbf{x}') / 2)$	$\ \Sigma_L^{-1}(\mathbf{x} - \mathbf{x}')\ $	$\sigma_f^2 \exp(-0.5)$
RQ	$\sigma_f^2 (1 + \ \mathbf{x} - \mathbf{x}'\ ^2 / (2\alpha\sigma_l^2))$	$\ \mathbf{x} - \mathbf{x}'\ $	$\frac{\sigma_f^2}{\sigma_l^2} (2\alpha(\alpha + 1) / (2\alpha^2 + 2\alpha - 1))^{-\alpha-1} \sqrt{\frac{2\alpha l^2}{2\alpha^2 + 2\alpha - 1}}$
Periodic	$\sigma_f^2 \left(1 + \frac{\ \mathbf{x} - \mathbf{x}'\ ^2}{2\alpha\sigma_l^2}\right)$	$\ \mathbf{x} - \mathbf{x}'\ $	$\begin{cases} \frac{4\pi\sigma_f^2}{p\sigma_l^2} \exp(-\frac{2}{\sigma_l^2}), & \text{if } \sigma_l^2 \geq 4 \\ \frac{2\pi\sigma_f^2}{p\sigma_l^2} \exp(-\frac{1}{2}), & \text{if } \sigma_l^2 < 4 \end{cases}$

Table I: Distance functions and Lipschitz constants of commonly used kernels, e.g., linear (LINEAR) kernel, squared exponential (SE) kernel, automatic relevance determination-squared exponential (ARD-SE) kernel, rational quadratic (RQ) kernel, and periodic (PERIODIC) kernel.

Therefore, when $\frac{d_x^2(x, x')}{l^2} = 1$, the Lipschitz constant of κ_{SE} is obtained as

$$L_{\kappa, SE} = \frac{\sigma_f^2}{\sigma_l} \exp(-\frac{1}{2}), \quad (28)$$

which concludes the proof.

B. Corollaries of the Other Lipschitz constant of Kernel

C. Lipschitz Continuity for ARD-SE Kernel

The distance function and the Lipschitz constant associated with ARD-SE kernel are given in the following corollary.

Corollary 1. Consider the ARD-SE kernel used and its distance function defined as

$$d_{ARD-SE}(\mathbf{x}, \mathbf{x}') = \|\Sigma_L^{-1}(\mathbf{x} - \mathbf{x}')\|, \quad \forall \mathbf{x}, \mathbf{x}' \in \mathbb{R}^n,$$

then the corresponding Lipschitz constant is $L_{\kappa, ARD-SE} = \sigma_f^2 \exp(-0.5)$.

Proof. Define an auxiliary variable ς as $\varsigma = \Sigma_L^{-1}(\mathbf{x} - \mathbf{x}')$, then the ARD-SE kernel is reformulated as $\kappa_{ARD-SE}(\mathbf{x}, \mathbf{x}') = \kappa_{SE}(\varsigma) = \sigma_f^2 \exp(-0.5\varsigma^T \varsigma)$, such that the derivative of $\kappa_{SE}(\mathbf{x}, \mathbf{x}')$ w.r.t \mathbf{x} is written as

$$\frac{d}{d\varsigma} \kappa_{SE}(\varsigma) = -\kappa_{SE}(\varsigma)\varsigma. \quad (29)$$

Moreover, the norm of the derivative is presented as

$$\left\| \frac{d}{d\varsigma} \kappa_{SE}(\varsigma) \right\| = \kappa_{SE}(\|\varsigma\|) \|\varsigma\|, \quad (30)$$

where the maximum of the right-hand side is achieved when $\|\varsigma\| = 1$ with the maximum as

$$\begin{aligned} \max_{\mathbf{x} \in \mathbb{R}^n} \left\| \frac{d}{d\varsigma} \kappa_{SE}(\varsigma) \right\| &= \max_{\varsigma \in \mathbb{R}^n} \kappa_{SE}(\|\varsigma\|) \|\varsigma\| \\ &= \sigma_f^2 \exp(-0.5) = L_{\kappa, ARD-SE}. \end{aligned} \quad (31)$$

Next, we consider the difference of ARD-SE kernel with different inputs as

$$\kappa_{ARD-SE}(\mathbf{x}, \mathbf{x}_1) - \kappa_{ARD-SE}(\mathbf{x}, \mathbf{x}_2) = \kappa_{SE}(\varsigma_1) - \kappa_{SE}(\varsigma_2) \quad (32)$$

with $\varsigma_1 = \Sigma_L^{-1}(\mathbf{x} - \mathbf{x}_1)$ and $\varsigma_2 = \Sigma_L^{-1}(\mathbf{x} - \mathbf{x}_2)$. Using the mean value theorem, the absolute value of the difference is written as

$$\begin{aligned} &|\kappa_{ARD-SE}(\mathbf{x}, \mathbf{x}_1) - \kappa_{ARD-SE}(\mathbf{x}, \mathbf{x}_2)| \\ &= \left| \left(\frac{d\kappa_{SE}(\varsigma^*)}{d\varsigma^*} \right)^T (\varsigma_1 - \varsigma_2) \right| \leq \left\| \frac{d\kappa_{SE}(\varsigma^*)}{d\varsigma^*} \right\| \|\varsigma_1 - \varsigma_2\| \end{aligned} \quad (33)$$

with $\varsigma^* = a\varsigma_1 + (1-a)\varsigma_2$ with $a \in [0, 1]$. Considering (31) and the fact $\|\varsigma_1 - \varsigma_2\| = d_x(\mathbf{x}_1, \mathbf{x}_2)$, the inequality

$$|\kappa_{ARD-SE}(\mathbf{x}, \mathbf{x}_1) - \kappa_{ARD-SE}(\mathbf{x}, \mathbf{x}_2)| \leq L_{\kappa, ARD-SE} d_x(\mathbf{x}_1, \mathbf{x}_2) \quad (34)$$

holds for any $\mathbf{x}, \mathbf{x}_1, \mathbf{x}_2 \in \mathbb{R}^n$, which concludes the proof. \square

D. Lipschitz Continuity for Linear Kernel

The distance function and the Lipschitz constant associated with Linear kernel are given in the following corollary.

Corollary 2. Consider the linear kernel defined by

$$\kappa_{Lin}(\mathbf{x}, \mathbf{x}') = \sigma_l^2(\mathbf{x} - \mathbf{c})^T(\mathbf{x}' - \mathbf{c}) + \sigma_b^2, \quad (35)$$

where σ_l is the hyper-parameter and the constant variance σ_b^2 determines how far from 0 the height of the function will be at zero. Choose the distance function as

$$d_{Lin}(\mathbf{x}, \mathbf{x}') = (\mathbf{x} - \mathbf{c})^T(\mathbf{x}' - \mathbf{c}), \quad \forall \mathbf{x}, \mathbf{x}' \in \mathbb{R}^n, \quad (36)$$

and consider the results in Lemma 3. Then the corresponding Lipschitz constant is written as

$$L_{\kappa, Lin} = \sigma_l^2. \quad (37)$$

Proof. The proof is straightforward and omitted for brevity. \square

E. Lipschitz Continuity for RQ Kernel

The distance function and the Lipschitz constant associated with RQ kernel are given in the following corollary.

Corollary 3. Consider the rational quadratic (RQ) kernel defined by

$$\kappa_{RQ}(\mathbf{x}, \mathbf{x}') = \sigma_f^2 \left(1 + \frac{\|\mathbf{x} - \mathbf{x}'\|^2}{2\alpha\sigma_l^2} \right), \quad (38)$$

where σ_f and σ_l are the hyper-parameters and the parameter $\alpha > 0$ governs the relative weighting of large-scale and small-scale variations. As α tends towards infinity, the RQ kernel converges to the SE kernel. Choose the distance function as

$$d_{RQ}(\mathbf{x}, \mathbf{x}') = \|\mathbf{x} - \mathbf{x}'\|, \quad \forall \mathbf{x}, \mathbf{x}' \in \mathbb{R}^n, \quad (39)$$

and consider the results in Lemma 3. Then the corresponding Lipschitz constant is written as

$$L_{\kappa, RQ} = \frac{\sigma_f^2}{\sigma_l^2} \left(\frac{2\alpha^2 + 2\alpha}{2\alpha^2 + 2\alpha - 1} \right)^{-\alpha-1} \sqrt{\frac{2\alpha l^2}{2\alpha^2 + 2\alpha - 1}}. \quad (40)$$

Proof. The proof follows Corollary 1. We first derive the derivative of κ_{RQ} w.r.t d_{RQ} as

$$\begin{aligned} & \nabla_{d_{RQ}(\mathbf{x}, \mathbf{x}')}\kappa_{RQ}(\mathbf{x}, \mathbf{x}') \\ &= -\sigma^2 \left(1 + \frac{d_{RQ}^2(\mathbf{x}, \mathbf{x}')}{2\alpha\sigma_l^2}\right)^{-\alpha-1} \left(\frac{d_{RQ}(\mathbf{x}, \mathbf{x}')}{\sigma_l^2}\right). \end{aligned} \quad (41)$$

According to the second derivative

$$\begin{aligned} & \nabla_{d_{RQ}(\mathbf{x}, \mathbf{x}')}\left(|\nabla_{d_{RQ}(\mathbf{x}, \mathbf{x}')}\kappa_{RQ}(\mathbf{x}, \mathbf{x}')|\right) \\ &= \nabla_{d_{RQ}(\mathbf{x}, \mathbf{x}')}\left(\sigma_f^2 \left(1 + \frac{d_{RQ}^2(\mathbf{x}, \mathbf{x}')}{2\alpha\sigma_l^2}\right)^{-\alpha-1} \left(\frac{d_{RQ}(\mathbf{x}, \mathbf{x}')}{\sigma_l^2}\right)\right) \\ &= \left(-(\alpha+1) \frac{\sigma_f^2}{\sigma_l^2} \left(1 + \frac{d_{RQ}^2(\mathbf{x}, \mathbf{x}')}{2\alpha\sigma_l^2}\right)^{-\alpha-2} \left(\frac{d_{RQ}(\mathbf{x}, \mathbf{x}')}{\sigma_l^2}\right)\right) \\ & \quad + \left(\frac{\sigma_f^2}{\sigma_l^2} \left(1 + \frac{d_{RQ}^2(\mathbf{x}, \mathbf{x}')}{2\alpha\sigma_l^2}\right)^{-\alpha-1}\right) \\ &= \frac{\sigma_f^2}{\sigma_l^2} \left(1 + \frac{d_{RQ}^2(\mathbf{x}, \mathbf{x}')}{2\alpha\sigma_l^2}\right)^{-\alpha-1} \\ & \quad \times \left(1 - (\alpha+1) \left(1 + \frac{d_{RQ}^2(\mathbf{x}, \mathbf{x}')}{2\alpha\sigma_l^2}\right)^{-1} \left(\frac{d_{RQ}^2(\mathbf{x}, \mathbf{x}')}{\sigma_l^2}\right)\right), \end{aligned} \quad (42)$$

then the maximum of $|\nabla_{d_{RQ}(\mathbf{x}, \mathbf{x}')}\kappa_{RQ}(\mathbf{x}, \mathbf{x}')|$ is achieved when

$$(\alpha+1) \left(1 + \frac{d_{RQ}^2(\mathbf{x}, \mathbf{x}')}{2\alpha\sigma_l^2}\right)^{-1} \left(\frac{d_{RQ}^2(\mathbf{x}, \mathbf{x}')}{\sigma_l^2}\right) = 1. \quad (43)$$

Therefore,

$$L_{\kappa, RQ} = \frac{\sigma_f^2}{\sigma_l^2} \left(\frac{2\alpha^2 + 2\alpha}{2\alpha^2 + 2\alpha - 1}\right)^{-\alpha-1} \sqrt{\frac{2\alpha\sigma_l^2}{2\alpha^2 + 2\alpha - 1}}. \quad (44)$$

This concludes the proof. \square

F. Lipschitz Continuity for Periodic Kernel

The distance function and the Lipschitz constant associated with periodic kernel are given in the following corollary.

Corollary 4. Consider the periodic kernel defined by

$$\kappa_{Per}(\mathbf{x}, \mathbf{x}') = \sigma_f^2 \exp\left(-\frac{2 \sin\left(\frac{\pi\|\mathbf{x}-\mathbf{x}'\|}{p}\right)}{\sigma_l^2}\right), \quad (45)$$

where σ_f and σ_l are the hyper-parameters and the period $p > 0$ determines the distance between repetitions of the function. Choose the distance function as

$$d_{Per}(\mathbf{x}, \mathbf{x}') = \|\mathbf{x} - \mathbf{x}'\|, \quad \forall \mathbf{x}, \mathbf{x}' \in \mathbb{R}^n, \quad (46)$$

and consider the results in Lemma 3. Then the corresponding Lipschitz constant is written as

$$L_{\kappa, Per} = \begin{cases} \frac{4\pi\sigma_f^2}{p\sigma_l^2} \exp(-\frac{2}{\sigma_l^2}), & \text{if } \sigma_l^2 \geq 4 \\ \frac{2\pi\sigma_f^2}{p\sigma_l} \exp(-\frac{1}{2}), & \text{if } \sigma_l^2 < 4 \end{cases}. \quad (47)$$

Proof. Similar to Corollary 1, the derivative of κ_{Per} w.r.t d_{Per} is

$$\begin{aligned} & \nabla_{d_x(\mathbf{x}, \mathbf{x}')}\kappa_{Per}(\mathbf{x}, \mathbf{x}') = -4 \sin\left(\pi \frac{d_{Per}(\mathbf{x}, \mathbf{x}')}{p}\right) \\ & \quad \times \left(\frac{\pi\sigma_f^2}{p\sigma_l^2}\right) \exp\left(-\frac{2 \sin^2\left(\pi \frac{d_{Per}(\mathbf{x}, \mathbf{x}')}{p}\right)}{\sigma_l^2}\right). \end{aligned} \quad (48)$$

To facilitate the derivation, we define $s(\mathbf{x}, \mathbf{x}') = \sin(\pi\|\mathbf{x} - \mathbf{x}'\|/p)$. Then the derivative of Eq. (48) w.r.t $s(\mathbf{x}, \mathbf{x}')$ is written as

$$\begin{aligned} & \nabla_{s(\mathbf{x}, \mathbf{x}')}\left(|\nabla_{d_{Per}(\mathbf{x}, \mathbf{x}')}\kappa_{Per}(\mathbf{x}, \mathbf{x}')|\right) \\ &= \nabla_{\sin\left(\pi \frac{\|\mathbf{x}-\mathbf{x}'\|}{p}\right)}\left(\exp\left(-\frac{2s^2(\mathbf{x}, \mathbf{x}')}{\sigma_l^2}\right) 4s(\mathbf{x}, \mathbf{x}') \left(\frac{\pi\sigma_f^2}{p\sigma_l^2}\right)\right) \\ &= \left(-\frac{4\pi\sigma_f^2}{p\sigma_l^2} \exp\left(-\frac{2s^2(\mathbf{x}, \mathbf{x}')}{\sigma_l^2}\right) \frac{4s(\mathbf{x}, \mathbf{x}')}{\sigma_l^2} s(\mathbf{x}, \mathbf{x}')\right) \\ & \quad + \left(\frac{4\pi\sigma_f^2}{p\sigma_l^2} \exp\left(-\frac{2s^2(\mathbf{x}, \mathbf{x}')}{\sigma_l^2}\right)\right) \\ &= \frac{4\pi\sigma_f^2}{p\sigma_l^2} \exp\left(-\frac{2s^2(\mathbf{x}, \mathbf{x}')}{\sigma_l^2}\right) \left(-\frac{4s^2(\mathbf{x}, \mathbf{x}')}{\sigma_l^2} + 1\right). \end{aligned} \quad (49)$$

If $\frac{\sigma_l^2}{4} \geq 1$, one has

$$1 - \frac{4s(\mathbf{x}, \mathbf{x}')}{\sigma_l^2} \geq 1 - \frac{4}{\sigma_l^2} \geq 0 \quad (50)$$

due to the fact $s(\mathbf{x}, \mathbf{x}') \geq 1$. Therefore, the maximum of $|\nabla_{d_{Per}(\mathbf{x}, \mathbf{x}')}\kappa_{Per}(\mathbf{x}, \mathbf{x}')|$ locating at $s(\mathbf{x}, \mathbf{x}') = 1$ is

$$\max |\nabla_{d_{Per}(\mathbf{x}, \mathbf{x}')}\kappa_{Per}(\mathbf{x}, \mathbf{x}')| = \frac{4\pi\sigma_f^2}{p\sigma_l^2} \exp\left(-\frac{2}{\sigma_l^2}\right). \quad (51)$$

If $\frac{\sigma_l^2}{4} < 1$, then the maximum of $|\nabla_{d_{Per}(\mathbf{x}, \mathbf{x}')}\kappa_{Per}(\mathbf{x}, \mathbf{x}')|$ locating at $s(\mathbf{x}, \mathbf{x}') = \frac{1}{2}$ is

$$\max |\nabla_{d_{Per}(\mathbf{x}, \mathbf{x}')}\kappa_{Per}(\mathbf{x}, \mathbf{x}')| = \frac{2\pi\sigma_f^2}{p\sigma_l} \exp\left(-\frac{1}{2}\right), \quad (52)$$

which concludes the proof. \square

V. ADDITIONAL SIMULATION RESULTS

A. Simulation Configuration

The codes are executed in MATLAB R2021b on the laptop with AMD Ryzen 7 5800H with 16.0GB RAM using MediaTek Wi-Fi 6 MT7921 Wireless LAN Card.

B. Regression Tasks

In the GPgym platform, we employ a default configuration featuring 4 Gaussian Process (GP) models, with their parameters detailed in Table II. The time interval for the exchange of input \mathbf{x} and the reception of predictions is set at 0.02 seconds to and from all distributed GPs with the centralized node. We utilize the ARD-SE kernel with optimized hyperparameters obtained from the full dataset. Moreover, the listening frequency for all GP models is established at 1000 Hz, and

Properties	GP model 1	GP model 2	GP model 3	GP model 4
Maximal Number of data samples	100	50	500	1000
Maximal Number of local GP models	100	200	50	20
Overlap Rate	0.01	0.01	0.01	0.01

Table II: Parameters for distributed LoG-GP

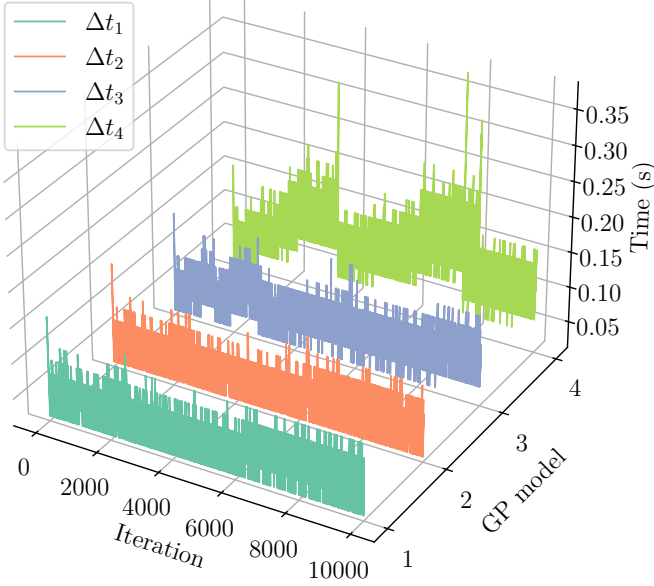


Figure 1: The delay time of the results of GP models.

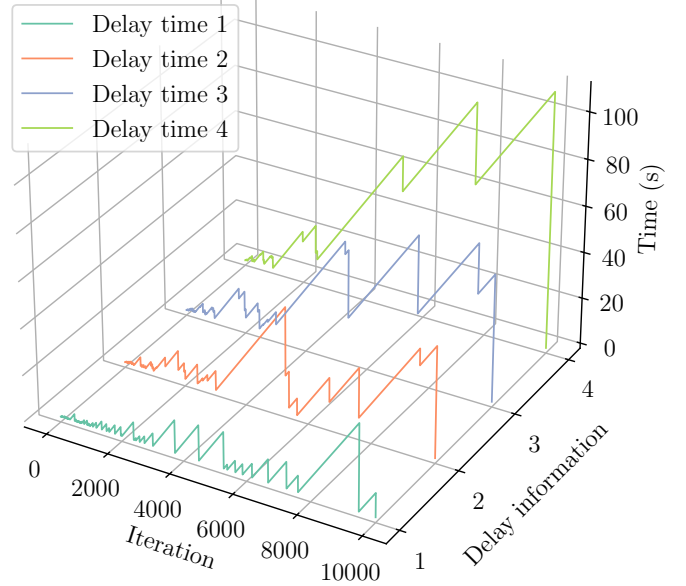


Figure 2: The sorted delay time of the results in the information set of AsyncDGP.

predictions are promptly relayed back to the centralized node upon generation.

In the first example, we set the information set threshold \bar{J} to be 4. The objective is to assess the performance of existing approaches in asynchronous prediction. This is particularly relevant as current approaches solely aggregate the most recent results from the GP models. Consequently, the information set consistently comprises 4 results sets, i.e., \mathbb{P}_i ($i = 1, \dots, 4$). Moreover, we provide the additional result of the delay time for the datasets SARCOS and PUMADYN32NM in Fig. 3 and 4, respectively.

In Fig. 1, the temporal delay Δt_i relative to the current time of used results of GP model i ($i = 1, 2, 3, 4$) on the KIN40K dataset is shown. It is noteworthy that, given the existing methods only utilize the most recent results, the delay time Δt_i is inherently identical to the delay time of results in the information set. Conversely, with AsyncDGP, where the results in the information set are composed of previous iterations, the sorted delay time of previous results is presented in Fig. 2 for the case where $\bar{J} = 4$. Specially, during the interval wherein the delay time of used results is consistently increasing, each model incorporates previous results in its utilization.

Additionally, we present a scenario with $\bar{J} = 10$, wherein the central node can aggregate more results to infer the unknown functions. To align with this objective and enable similar functionality for other approaches, we have devised the aggregation strategies for the 5 existing distributed methods, which are formulated as follows.

- Bayesian committee machine (BCM):

$$\hat{f}(\mathbf{x}(t)) = \sum_{i=1}^M \sum_{k=0}^{\bar{k}_i(t)} \omega_k^i(t) \mu_i(\mathbf{x}(t_i^k)) + \omega_m(t) m(\mathbf{x}(t)), \quad (53)$$

with the aggregation weights

$$\begin{aligned} \omega_k^i(t) &= \omega^2(t) \sigma_i^{-2}(\mathbf{x}(t_i^k)), \\ \omega_m(t) &= \omega^2(t) (1 - \rho(t)) \sigma_f^{-2}, \end{aligned} \quad (54)$$

where

$$\rho(t) = \sum_{i=1}^M (\bar{k}_i(t) + 1), \quad (55)$$

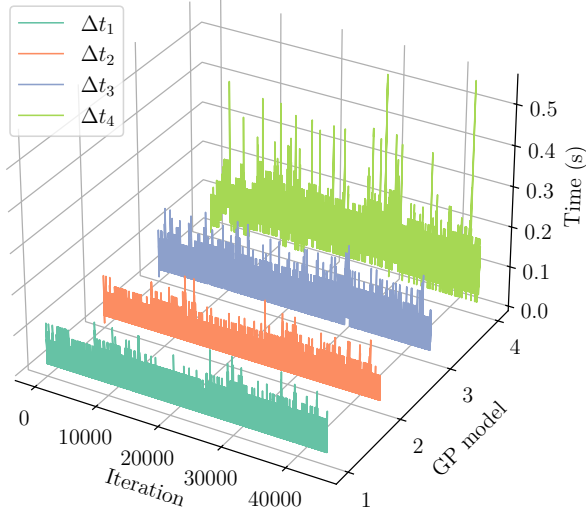
$$\omega^{-2}(t) = \sum_{i=1}^M \sum_{k=0}^{\bar{k}_i(t)} \sigma_i^{-2}(\mathbf{x}(t_i^k)) + (1 - \rho(t)) \sigma_f^{-2}.$$

- Robust Bayesian committee machine (rBCM):

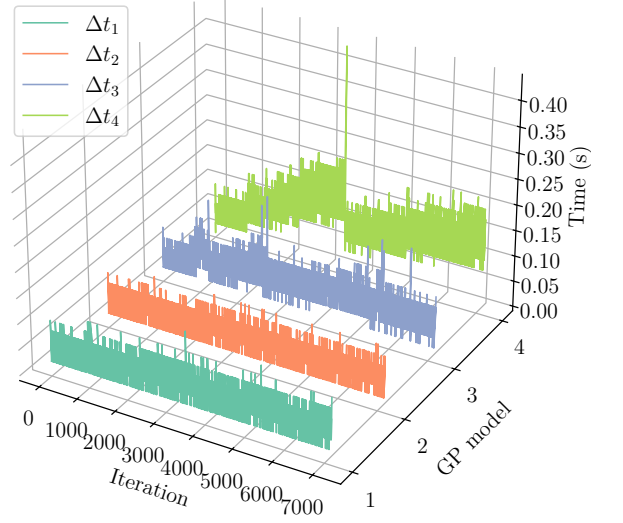
$$\hat{f}(\mathbf{x}(t)) = \sum_{i=1}^M \sum_{k=0}^{\bar{k}_i(t)} \omega_k^i(t) \mu_i(\mathbf{x}(t_i^k)) + \omega_m(t) m(\mathbf{x}(t)), \quad (56)$$

with the aggregation weights

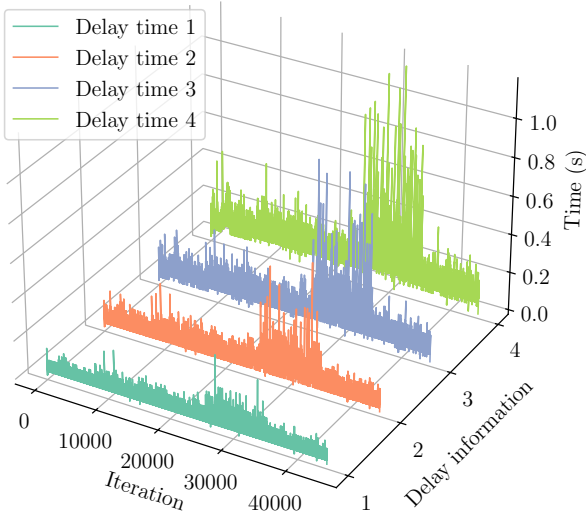
$$\begin{aligned} \omega_k^i(t) &= \omega^2(t) \rho_k^i(t) \sigma_i^{-2}(\mathbf{x}(t_i^k)), \\ \omega_m(t) &= \omega^2(t) (1 - \rho(t)) \sigma_f^{-2}, \end{aligned} \quad (57)$$



(a) The delay time of the results of GP models.

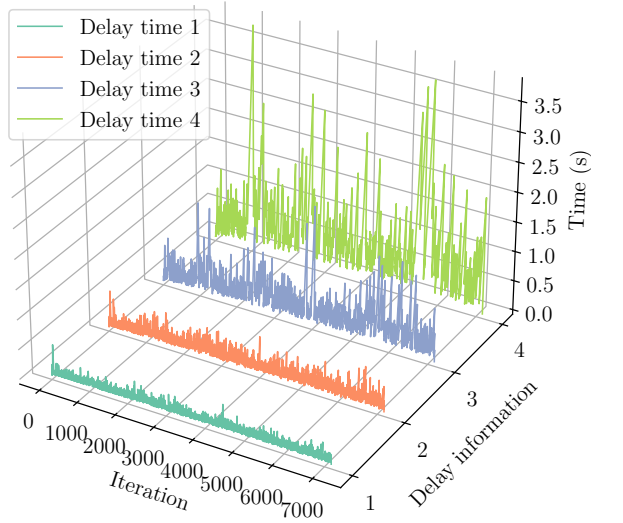


(a) The delay time of the results of GP models.



(b) The delay time of the results in the information set.

Figure 3: The delay time of the results on SARCOS.



(b) The delay time of the results in the information set.

Figure 4: The delay time of the results on PUMADYN32NM.

where $\rho(t) = \sum_{i=1}^M \sum_{k=0}^{\bar{k}_i(t)} \rho_k^i(t)$ and

$$\begin{aligned} \rho_k^i(t) &= \log(\sigma_f / \sigma_i(\mathbf{x}(t_i^k))), \quad \omega^{-2}(t) \\ &= \sum_{i=1}^M \sum_{k=0}^{\bar{k}_i(t)} \rho_k^i(t) \sigma_i^{-2}(\mathbf{x}(t_i^k)) + (1 - \rho(t)) \sigma_f^{-2}. \end{aligned} \quad (58)$$

- Product-of-experts (POE):

$$\hat{f}(\mathbf{x}(t)) = \sum_{i=1}^M \sum_{k=0}^{\bar{k}_i(t)} \omega_k^i(t) \mu_i(\mathbf{x}(t_i^k)), \quad (59)$$

with the aggregation weights $\omega_k^i(t) = \omega^2(t) \sigma_i^{-2}(\mathbf{x}(t_i^k))$, where $\omega^{-2}(t) = \sum_{i=1}^M \sum_{k=0}^{\bar{k}_i(t)} \sigma_i^{-2}(\mathbf{x}(t_i^k))$.

- Generalized product-of-experts (gPOE):

$$\hat{f}(\mathbf{x}(t)) = \sum_{i=1}^M \sum_{j=0}^{\bar{k}_i(t)} \omega_k^i(t) \mu_i(\mathbf{x}(t_i^k)), \quad (60)$$

with the aggregation weights $\omega_k^i(t)$ defined as $\omega_k^i(t) =$

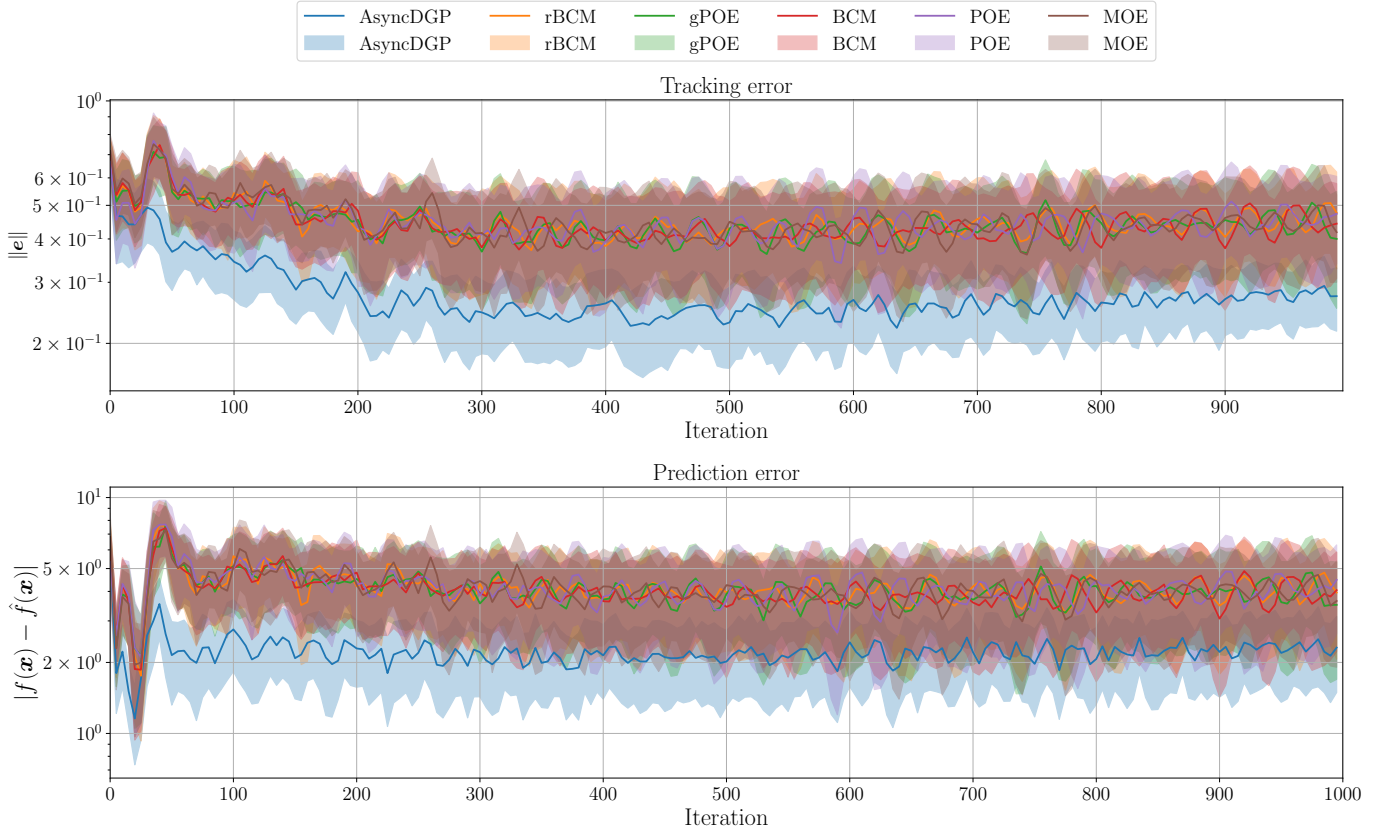


Figure 5: The prediction errors and tracking errors over 1000 iterations.

$$\omega^2(t)\rho_k^i(t)\sigma_i^{-2}(\mathbf{x}(t_i^k)), \text{ where}$$

$$\rho_k^i(t) = \log(\sigma_f/\sigma_i(\mathbf{x}(t_i^k))), \quad (61)$$

$$\omega^{-2}(t) = \sum_{i=1}^M \sum_{k=0}^{\bar{k}_i(t)} \rho_k^i(t)\sigma_i^{-2}(\mathbf{x}(t_i^k)).$$

- Mixture of experts (MOE):

$$\hat{f}(\mathbf{x}(t)) = \frac{\sum_{i=1}^M \sum_{k=0}^{\bar{k}_i(t)} \mu_i(\mathbf{x}(t_i^k))}{\sum_{i=1}^M \sum_{k=0}^{\bar{k}_i(t)} 1}. \quad (62)$$

C. Control Tasks

In the control task, a total of 1000 training samples are uniformly distributed in the domain $[-3, 3] \times [-3, 3]$. We conduct 100 simulations over a duration of 20 seconds each, employing state broadcasting and listening with a fixed time interval of 0.02 seconds. The initial states are evenly sampled in $[0, 1] \times [0, 1]$, and the reference follows a uniform distribution between $[0.4, 0.6]$ and $[3, 5]$ for each simulation, respectively. To demonstrate the control performance during over 100 Monte-Carlo simulations, Fig. 5 shows the mean values (solid line) and its variance (light shade) in the 1000 iterations. Moreover, the statistical results are shown in Fig. 6.

ACKNOWLEDGMENTS

This work has been financially supported by the Federal Ministry of Education and Research of Germany in the programme of ‘‘Souverän. Digital. Vernetzt.’’ under joint project

6G-life with project identification number: 16KISK002, and by the European Research Council (ERC) Consolidator Grant ‘‘Safe data-driven control for human-centric systems (CO-MAN)’’ under grant agreement number 864686.

REFERENCES

- [1] X. D. Zewen Yang and S. Hirche, ‘‘Asynchronous distributed gaussian process regression,’’ in *The 39th Annual AAAI Conference on Artificial Intelligence*, 2024. [Online]. Available: <https://openreview.net/forum?id=Ok1B7DL8ZO>
- [2] X. Dai, A. Lederer, Z. Yang, and S. Hirche, ‘‘Can Learning Deteriorate Control? Analyzing Computational Delays in Gaussian Process-Based Event-Triggered Online Learning,’’ in *Learning for Dynamics and Control Conference*. PMLR, 2023, pp. 445–457.
- [3] E. Snelson and Z. Ghahramani, ‘‘Sparse gaussian processes using pseudo-inputs,’’ *Advances in neural information processing systems*, vol. 18, 2005.
- [4] M. Titsias, ‘‘Variational learning of inducing variables in sparse gaussian processes,’’ in *Artificial intelligence and statistics*. PMLR, 2009, pp. 567–574.
- [5] A. Melkumyan and F. T. Ramos, ‘‘A sparse covariance function for exact gaussian process inference in large datasets,’’ in *Twenty-first international joint conference on artificial intelligence*, 2009.
- [6] A. Nayebi, A. Munteanu, and M. Poloczek, ‘‘A framework for bayesian optimization in embedded subspaces,’’ in *International Conference on Machine Learning*. PMLR, 2019, pp. 4752–4761.
- [7] H. Liu, Y.-S. Ong, X. Shen, and J. Cai, ‘‘When Gaussian Process Meets Big Data: A Review of Scalable GPs,’’ vol. 31, no. 11, pp. 4405–4423, 2020.
- [8] M. Jiang, G. Pedrielli, and S. H. Ng, ‘‘Gaussian processes for high-dimensional, large data sets: A review,’’ in *2022 Winter Simulation Conference (WSC)*. IEEE, 2022, pp. 49–60.

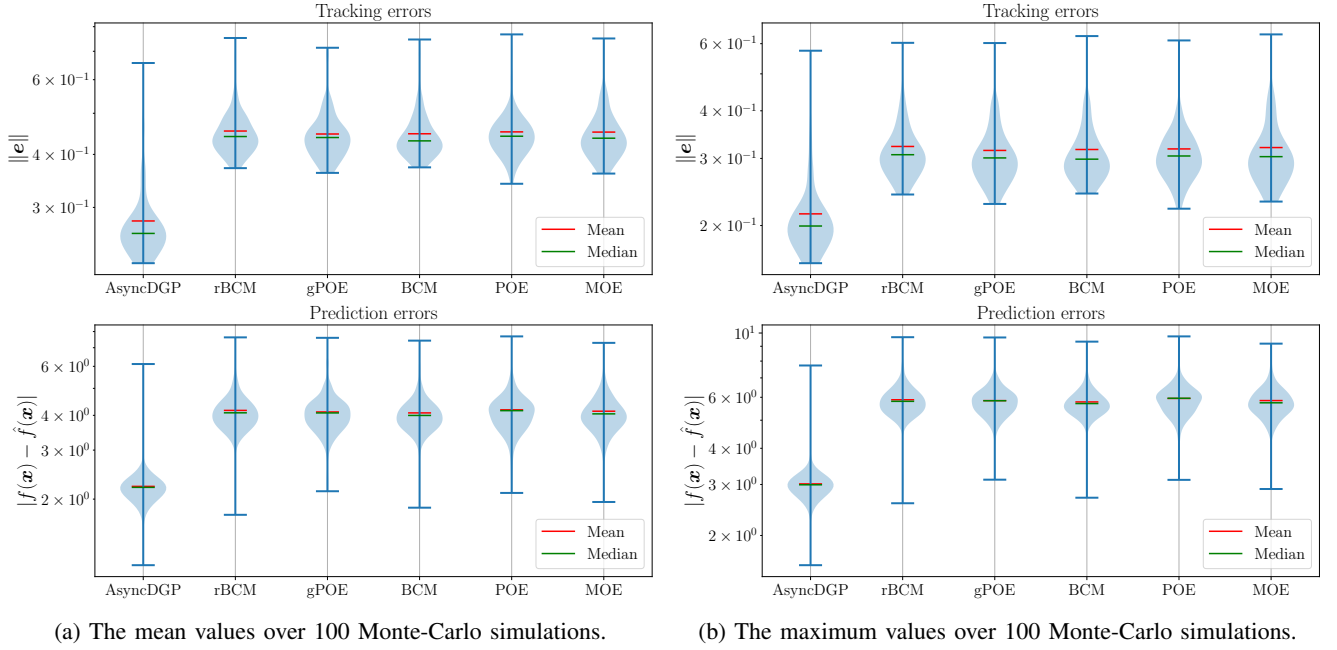


Figure 6: The violin plots for mean and maximum values of the Monte-Carlo simulation.

- [9] V. Tresp, "Mixtures of Gaussian Processes," in *Advances in Neural Information Processing Systems*, T. Leen, T. Dietterich, and V. Tresp, Eds., vol. 13. MIT Press, 2000. [Online]. Available: https://proceedings.neurips.cc/paper_files/paper/2000/file/9fdb62f932adf55af2c0e09e55861964-Paper.pdf
- [10] C. Yuan and C. Neubauer, "Variational mixture of gaussian process experts," *Advances in neural information processing systems*, vol. 21, 2008.
- [11] S. Masoudnia and R. Ebrahimpour, "Mixture of Experts: A Literature Survey," vol. 42, no. 2, pp. 275–293, 2014. [Online]. Available: <http://link.springer.com/10.1007/s10462-012-9338-y>
- [12] G. E. Hinton, "Training Products of Experts by Minimizing Contrastive Divergence," *Neural Computation*, vol. 14, no. 8, pp. 1771–1800, 2002.
- [13] J. W. Ng and M. P. Deisenroth, "Hierarchical Mixture-of-Experts Model for Large-Scale Gaussian Process Regression," 2014.
- [14] Y. Cao and D. J. Fleet, "Generalized Product of Experts for Automatic and Principled Fusion of Gaussian Process Predictions," 2015. [Online]. Available: <http://arxiv.org/abs/1410.7827>
- [15] S. Cohen, R. Mubvha, T. Marwala, and M. Deisenroth, "Healing Products of Gaussian Process Experts," in *Proceedings of the 37th International Conference on Machine Learning*, ser. Proceedings of Machine Learning Research, H. D. III and A. Singh, Eds., vol. 119. PMLR, 13–18 Jul 2020, pp. 2068–2077. [Online]. Available: <https://proceedings.mlr.press/v119/cohen20b.html>
- [16] M. Schürch, D. Azzimonti, A. Benavoli, and M. Zaffalon, "Correlated product of experts for sparse gaussian process regression," *Machine Learning*, pp. 1–22, 2023.
- [17] V. Tresp, "A Bayesian committee machine," *Neural computation*, vol. 12, no. 11, pp. 2719–2741, 2000.
- [18] M. Deisenroth and J. W. Ng, "Distributed Gaussian Processes," in *Proceedings of the 32nd International Conference on Machine Learning*, ser. Proceedings of Machine Learning Research, F. Bach and D. Blei, Eds., vol. 37. Lille, France: PMLR, 07–09 Jul 2015, pp. 1481–1490. [Online]. Available: <https://proceedings.mlr.press/v37/deisenroth15.html>
- [19] H. Liu, J. Cai, Y. Wang, and Y. S. Ong, "Generalized robust bayesian committee machine for large-scale gaussian process regression," in *International Conference on Machine Learning*. PMLR, 2018, pp. 3131–3140.
- [20] D. Rullière, N. Durrande, F. Bachoc, and C. Chevalier, "Nested Kriging predictions for datasets with a large number of observations," *Statistics and Computing*, vol. 28, pp. 849–867, 2018.
- [21] G. P. Kontoudis and D. J. Stilwell, "Decentralized nested gaussian processes for multi-robot systems," in *2021 IEEE International Conference on Robotics and Automation (ICRA)*, 2021, pp. 8881–8887.
- [22] Z. Yang, S. Dong, A. Lederer, X. Dai, S. Chen, S. Sosnowski, G. Hattab, and S. Hirche, "Cooperative Learning with Gaussian Processes for Euler-Lagrange Systems Tracking Control Under Switching Topologies," in *2024 American Control Conference (ACC)*, 2024, pp. 560–567.
- [23] Z. Yang, X. Dai, A. Dubey, S. Hirche, and G. Hattab, "Whom to Trust? Elective Learning for Distributed Gaussian Process Regression," in *Proceedings of the 23rd International Conference on Autonomous Agents and Multiagent Systems*, ser. AAMAS '24, 2024, p. 2020–2028.
- [24] Z. Yang, S. Sosnowski, Q. Liu, J. Jiao, A. Lederer, and S. Hirche, "Distributed Learning Consensus Control for Unknown Nonlinear Multi-Agent Systems based on Gaussian Processes," in *2021 60th IEEE Conference on Decision and Control (CDC)*. IEEE, 2021, pp. 4406–4411.
- [25] A. Lederer, Z. Yang, J. Jiao, and S. Hirche, "Cooperative Control of Uncertain Multiagent Systems via Distributed Gaussian Processes," *IEEE Transactions on Automatic Control*, vol. 68, no. 5, pp. 3091–3098, 2023.
- [26] T. N. Hoang, Q. M. Hoang, K. H. Low, and J. How, "Collective online learning of gaussian processes in massive multi-agent systems," in *Proceedings of the AAAI Conference on Artificial Intelligence*, vol. 33, no. 01, 2019, pp. 7850–7857.
- [27] Z. Yin, X. Dai, Z. Yang, Y. Shen, G. Hattab, and H. Zhao, "Learning-based Control for PMSM Using Distributed Gaussian Processes with Optimal Aggregation Strategy," in *IECON 2023- 49th Annual Conference of the IEEE Industrial Electronics Society*, 2023, pp. 1–7.
- [28] S. He, M. Tang, J. Fu, and J. Liang, "Distributed Online Sparse Gaussian Process Regression for Multi-Agent Coverage Control," in *2023 42nd Chinese Control Conference (CCC)*. IEEE, 2023, pp. 5464–5469. [Online]. Available: <https://ieeexplore.ieee.org/document/10239920/>
- [29] X. Dai, Z. Yang, S. Zhang, D.-H. Zhai, Y. Xia, and S. Hirche, "Cooperative Online Learning for Multiagent System Control via Gaussian Processes With Event-Triggered Mechanism," *IEEE Transactions on Neural Networks and Learning Systems*, pp. 1–15, 2024.
- [30] X. Dai, Z. Yang, M. Xu, S. Zhang, F. Liu, G. Hattab, and S. Hirche, "Decentralized event-triggered online learning for safe consensus control of multi-agent systems with Gaussian process regression," *European Journal of Control*, vol. 80, p. 101058, 2024. [Online]. Available: <https://www.sciencedirect.com/science/article/pii/S0947358024001183>
- [31] J. Chen, K. H. Low, Y. Yao, and P. Jaillet, "Gaussian process decentralized data fusion and active sensing for spatiotemporal traffic modeling and prediction in mobility-on-demand systems," *IEEE Transactions on Automation Science and Engineering*, vol. 12, no. 3, pp. 901–921, 2015.
- [32] R. Ouyang and B. K. H. Low, "Gaussian process decentralized data fusion meets transfer learning in large-scale distributed cooperative perception," *Autonomous Robots*, vol. 44, pp. 359–376, 2020.

- [33] G. P. Kontoudis and D. J. Stilwell, "Decentralized nested gaussian processes for multi-robot systems," in *2021 IEEE International Conference on Robotics and Automation (ICRA)*. IEEE, 2021, pp. 8881–8887.
- [34] G. Pillonetto, L. Schenato, and D. Varagnolo, "Distributed multi-agent gaussian regression via finite-dimensional approximations," *IEEE Transactions on Pattern Analysis and Machine Intelligence*, vol. 41, no. 9, pp. 2098–2111, 2018.
- [35] M. Tavassolipour, S. A. Motahari, and M. T. M. Shalmani, "Learning of gaussian processes in distributed and communication limited systems," *IEEE transactions on pattern analysis and machine intelligence*, vol. 42, no. 8, pp. 1928–1941, 2019.
- [36] H. Jalali and G. Kasneci, "Aggregating dependent gaussian experts in local approximation," in *2020 25th International Conference on Pattern Recognition (ICPR)*. IEEE, 2021, pp. 9015–9022.
- [37] Y.-C. Zhi, Y. C. Ng, and X. Dong, "Gaussian processes on graphs via spectral kernel learning," *IEEE Transactions on Signal and Information Processing over Networks*, vol. 9, pp. 304–314, 2023.
- [38] Y. Xu, J. Choi, and S. Oh, "Mobile sensor network navigation using gaussian processes with truncated observations," *IEEE Transactions on Robotics*, vol. 27, no. 6, pp. 1118–1131, 2011.
- [39] D. Jang, J. Yoo, C. Y. Son, D. Kim, and H. J. Kim, "Multi-Robot Active Sensing and Environmental Model Learning With Distributed Gaussian Process," *IEEE Robotics and Automation Letters*, vol. 5, no. 4, pp. 5905–5912, 2020.
- [40] W. Luo and K. Sycara, "Adaptive Sampling and Online Learning in Multi-Robot Sensor Coverage with Mixture of Gaussian Processes," in *2018 IEEE International Conference on Robotics and Automation (ICRA)*, 2018, pp. 6359–6364.
- [41] T. Ding, R. Zheng, S. Zhang, and M. Liu, "Resource-Efficient Cooperative Online Scalar Field Mapping Via Distributed Sparse Gaussian Process Regression," *IEEE Robotics and Automation Letters*, pp. 1–8, 2024.
- [42] K. Hashimoto, A. Saoud, M. Kishida, T. Ushio, and D. V. Dimarogonas, "Learning-based Symbolic Abstractions for Nonlinear Control Systems," *Automatica*, vol. 146, p. 110646, 2022.
- [43] D. S. Bernstein, *Matrix Mathematics: Theory, Facts, and Formulas*. Princeton university press, 2009.